

A Naphthalimide-Based Fluorescent Probe for the Detection and Imaging of Mercury Ions in Living Cells

Shaoyu Lei,^[a] Xia Meng,^[a] Lizhen Wang,^[b] Jianhua Zhou,^[a] Dawei Qin,^{*,[a]} and Hongdong Duan.^{*,[a]}

The selective and efficient monitoring of mercury (Hg^{2+}) contamination found in the environment and ecosystem has been carried out. Thus, a new 1,8-naphthalimide-based fluorescent probe NADP for the detection of Hg^{2+} based on a fluorescence enhancement strategy has been designed and synthesized. The NADP probe can detect Hg^{2+} with high selectivity and sensitivity and a low detection limit of 13 nM.

The detection mechanism was based on a Hg^{2+} -triggered deprotection reaction, resulting in a dramatic change in fluorescence from colorless to green at physiological pH. Most importantly, biological investigation has shown that the NADP probe can be successfully applied to the monitoring of Hg^{2+} in living cells and zebrafish with low cytotoxicity.

1. Introduction

Mercury (Hg^{2+}) is an ubiquitous heavy-metal contaminant of the environment, which is easily absorbed by plants and can be accumulated in other organisms through the food chain.^[1–10] In animals, Hg^{2+} can prevent normal cellular function and generally induce severe health problems such as neural disorders, cognitive and motor disorders, kidney failure, abdominal pain, pink disease, DNA lesions, and even death. Due to the characteristic properties of Hg^{2+} , it can combine with thiol groups in enzymes and proteins by passing through the biofilm.^[11–17] Owing to the extremely hazardous properties of Hg^{2+} , the U.S Environmental Protection Agency has explicitly stipulated that the maximum permissible level of mercury in drinking water should not exceed 2 ppb (10 nM).^[18] Thus, considering its persistence in the environment and high toxicity in living organisms,^[19–26] effective detection and disposal of Hg^{2+} are of great significance for environmental protection and public health.

Several traditional testing strategies have been well-established for the quantitative detection of Hg^{2+} , such as atomic absorption/emission spectroscopy,^[27–28] electrochemical analysis,^[29] surface-enhanced Raman scattering,^[30]

colorimetric,^[31] and inductively coupled plasma mass spectrometry.^[32] However, these conventional methods are commonly associated with drawbacks such as the need for sophisticated experimental equipment, professional technicians, long detection time, and can be cytotoxic, making them unsuitable for the detection of Hg^{2+} in living organisms. Recently, a great number of Hg^{2+} -selective fluorescent sensors have been designed with excellent sensitivity, low detection limit, convenient visual sensing, real-time monitoring, non-destructive testing, and applicability to biological analyses. Over the past decades, both Hg-ligand complexes and Hg-induced irreversible have been adopted for the detection of Hg^{2+} in biological and environmental systems.^[33–47] Many chelation-based probes for the determination of Hg^{2+} have been based on the on-off fluorescent type before and after analyte recognition, because Hg^{2+} acts as a fluorescence quenching agent by enhancing spin-orbit coupling. However, chelation-based probes were often affected by other metal ions with similar coordination properties.^[48–51] In contrast, an increasing number of reaction-based and fluorescence-enhanced probes have been developed based on the method of protection-deprotection and the ability of Hg^{2+} to promote desulfurization reactions to release fluorophores thus enhancing fluorescence.^[52–55] Therefore, it is highly urgent to develop sensitive and specific fluorescence enhanced probes based on Hg^{2+} -triggered specific reactions to detect Hg^{2+} in the environment and living cells.

Herein, considering the above factors, a simple yet efficient fluorescence enhanced probe NADP for the detection of Hg^{2+} has been developed based on a 1,3-dithiane moiety as the reaction site for Hg^{2+} and a 1,8-naphthalimide (NA-CHO) dye as a signal response fluorescent unit. This novel probe possesses desirable optical properties such as high photostability, a stable rigid structure and excellent biocompatibility. Once the reaction is triggered by Hg^{2+} , the NADP probe is converted to NA-CHO endowing it with enhanced fluorescence and a distinct color change from colorless to green. In addition, as a new probe, NADP displayed several advantages including

[a] S. Lei, X. Meng, Prof. J. Zhou, Prof. D. Qin, Prof. H. Duan.
School of Chemistry and Chemical Engineering
Qilu University of Technology (Shandong Academy of Sciences)
Ji'nan, Shandong Province, 250353, (China)
E-mail: daweiqin@163.com
hdduan67@163.com

[b] Dr. L. Wang
Biology Institute, Qilu University of Technology (Shandong Academy of Sciences)
Jinan 250103, Shandong Province (China)

Supporting information for this article is available on the WWW under <https://doi.org/10.1002/open.202100204>

© 2021 The Authors. Published by Wiley-VCH GmbH. This is an open access article under the terms of the Creative Commons Attribution Non-Commercial License, which permits use, distribution and reproduction in any medium, provided the original work is properly cited and is not used for commercial purposes.

fast response time, favorable anti-interference, and low detection limit in the detection of Hg^{2+} . Most importantly, NADP could be successfully applied to Hg^{2+} imaging with satisfactory results in living cells.

2. Results and Discussion

As shown in Figure 1a, the UV/Vis absorption spectrum of NADP in DMSO/PBS buffer (1:9, v/v, pH 7.4) shows absorption bands at 453 nm. However, significant changes took place in the UV/Vis absorption spectrum of NADP in DMSO/PBS buffer (1:9, v/v, pH 7.4) where absorption bands clearly changed from 453 to 415 nm with slight enhancement after simultaneous addition of Hg^{2+} was added, which was accompanied by a color change from yellow to pale yellow. The results of UV/Vis spectral data demonstrated that the NADP probe has the potential to be used for the development of specifically detectable probes for Hg^{2+} . Next, we explored the fluorescence emission spectrum of the NADP probe at an excitation wavelength of 400 nm. As displayed in Figure 1b, with the addition of mercury ions, it was found that the fluorescence intensity was remarkably enhanced and the fluorescent color changed from colorless to green, while the NADP probe showed a faint fluorescence emission

peak most likely because of the heavy atom effect.^[52] These findings revealed that NADP has the potential to become a colorimetric and fluorescent turn-on probe for monitoring Hg^{2+} .

To more clearly determine the sensitivity of NADP for Hg^{2+} , a fluorescence titration experiment of NADP toward different concentrations of Hg^{2+} was then carried out in DMSO/PBS buffer (1:9, v/v, pH 7.4). As demonstrated in Figure 2a, the NADP probe displayed a weak emission in DMSO/PBS buffer solution at 545 nm, while a remarkable green fluorescence emission band at 518 nm was gradually generated and enhanced with the increase of Hg^{2+} concentration. The fluorescence intensity reached a plateau when the concentration of Hg^{2+} was more than 1 equiv. Furthermore, the titration profile was utilized to evaluate the linear relationship between NADP and Hg^{2+} as the concentration increased from 0 to 10 μM . From the curve, it was clear that the fluorescence intensity of NADP displayed a preferable linear relationship ($R^2 = 0.99506$) toward Hg^{2+} concentrations Figure 2b, implying that the NADP probe can quantitatively and qualitatively determine Hg^{2+} . According to the equation $3\sigma/k$ (σ is the standard deviation of the blank solution; k is the slope of the calibration curve),^[56] the detection limit for NADP toward Hg^{2+} was calculated to be 13 nM. All of these results indicated that the NADP probe could sensitively monitor Hg^{2+} levels.

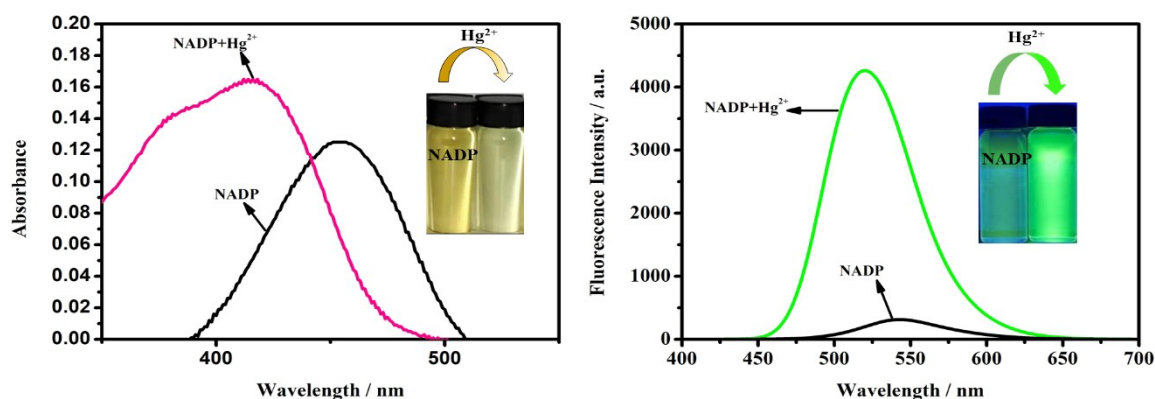


Figure 1. Absorption (a) and fluorescence emission (b) spectra of NADP (10 μM) with and without Hg^{2+} in DMSO/PBS buffer (1:9, v/v, pH 7.4). Inset: “Naked-eye” color changes of NADP (10 μM) in the presence of Hg^{2+} (20 μM) under room light and under a 365 nm UV lamp.

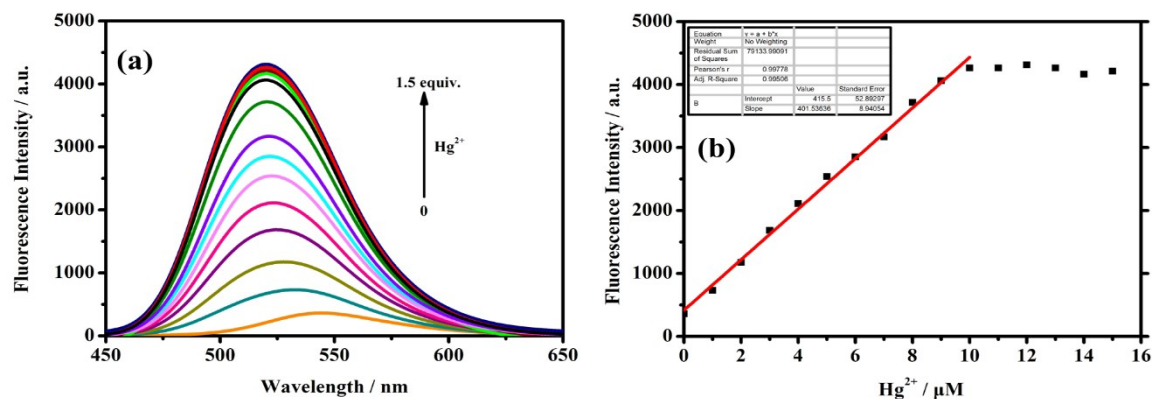
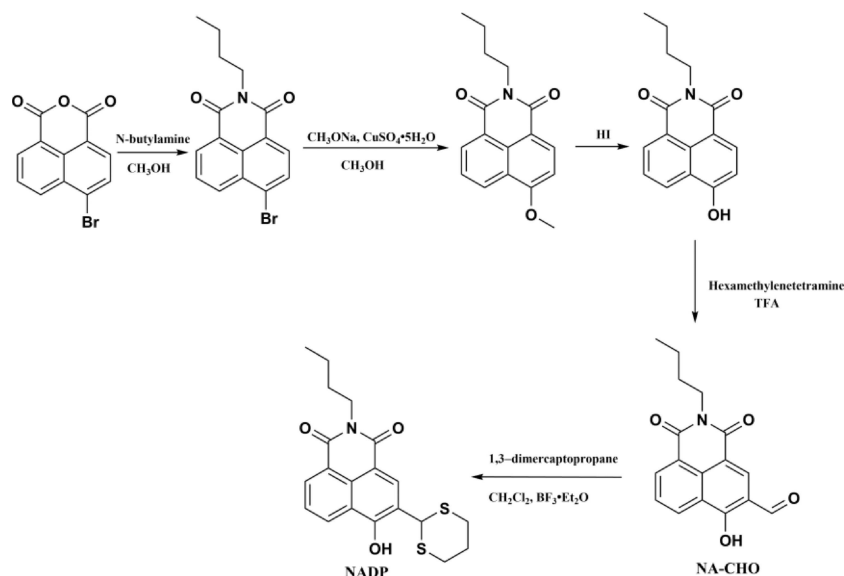


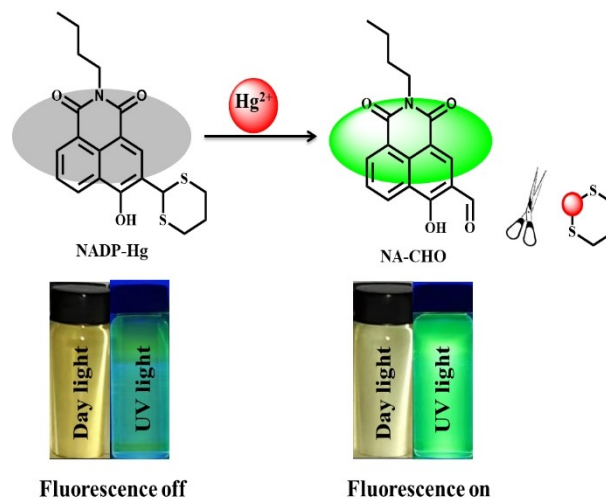
Figure 2. (a) Spectral changes in NADP (10 μM) exposed to various concentrations of Hg^{2+} (0–1.5 equiv) in DMSO/PBS buffer (1:9, v/v, pH 7.4); (b) Fluorescence intensity change in NADP with gradual addition of Hg^{2+} (0–1.5 equiv); Inset: Fluorescence images of NADP treated with Hg^{2+} .



Scheme 1. Synthesis of the NADP probe.

It has been proposed that the thioacetal portion of the NADP probe could be easily deprotected into an aldehyde group because alkyl thiols display high affinity with Hg^{2+} ,^[57] enabling the probe to be successfully converted into the compound NA-CHO based on the deprotection reaction of the dithioacetal triggered by Hg^{2+} . To further investigate the reaction mechanism of NADP with Hg^{2+} , ^1H NMR titration experiments were adopted to provide persuasive evidence. As exhibited in Figure S1 in the Supporting Information, it was found that the signal peak of the methine group (Hb) in the dithioacetal moiety of the NADP probe was seen at 5.57 ppm, while the aldehyde proton signal emerged at 10.13 ppm and was accompanied with a loss of the original proton signal at 5.57 ppm upon addition of Hg^{2+} . Furthermore, we can deduce that the thioacetal portion of the NADP probe has been successfully converted into an aldehyde group based on the deprotection reaction induced by Hg^{2+} , as the ^1H NMR spectra of the reaction for NADP with Hg^{2+} was very similar to those of the compound NA-CHO. In addition, high-resolution mass spectrometry was utilized to verify the reaction results of NADP with Hg^{2+} where a new prominent peak was displayed at $m/z = 298.1084$ [$\text{NADP} + \text{Hg}^{2+} + \text{H}$]⁺ (Figure S8 in the Supporting Information) corresponding to the compound NA-CHO. Considering the above results, a mechanism for the successful deprotection reaction is illustrated in Scheme 2.

We propose that the faint fluorescence of the probe may be due to the intramolecular charge transfer (ICT) process carried out between naphthalimide and 1,3-dithiane. To further make sense of the recognition mechanism of NADP in response to Hg^{2+} , the structures of NADP and NA-CHO were optimized by employing density functional theory with the $\omega\text{B97XD}/6\text{-311G}(\text{d,p})$ in a set of the Gaussian 09 programs.^[58–59] As displayed in Figure 3, the highest occupied molecular orbital (HOMO) of the NADP probe was centered on the phenyl moiety of naphthalimide and the part of the naphthalimide attached to the

Scheme 2. Proposed complexation model of NADP with Hg^{2+} .

dithioacetal, while the lowest unoccupied molecular orbital (LUMO) of the NADP probe was mostly dispersed over the phenyl moiety of naphthalimide. However, both the electron density of HOMO and LUMO of NA-CHO were congruently scattered in the entire molecular skeleton except for the carbon chain section, implying that there was no apparent intramolecular electron pushing-pulling phenomenon. The damage of the ICT procedure brought about a difference between the HOMO–LUMO energy gap of the NADP probe and NA-CHO. The HOMO–LUMO energy gap of the compound NA-CHO was 7.5540 eV higher than the energy gap of the NADP probe (7.4419 eV). These calculated results further verified the spectroscopic analysis and the detection mechanism for the NADP probe as revealed via the frontier molecular orbital theory.

To explore the selectivity of NADP toward Hg^{2+} , the fluorescence spectrum changes of NADP in the presence of

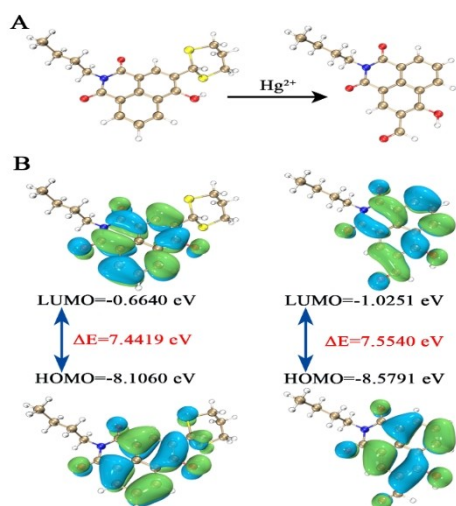


Figure 3. Frontier molecular orbitals of the NADP probe and compound NA-CHO.

environmental and biologically-related metal ions including K^+ , Ca^{2+} , Mg^{2+} , Al^{3+} , Na^+ , Fe^{3+} , Fe^{2+} , Hg^{2+} , Ag^+ , Cu^{2+} , Cr^{3+} , Cd^{2+} , Ni^{2+} , Co^{2+} , Pb^{2+} , and Zn^{2+} were measured in parallel under the same conditions. As depicted in Figure 4a, it was found that only the addition of Hg^{2+} to the probe solution resulted in a significant enhancement in fluorescence when various ions were added to the probe solution under the same conditions. Furthermore, it is rather remarkable that introduction of Ag^+ produced an emission enhancement and may contribute to the moderate coordination of Ag^+ with the sulfur atoms of the thioacetal moiety from the NADP probe.^[60] Furthermore, the potential interference of Ag^+ could be inhibited in a PBS

solution.^[61] In addition, it is of great importance when detecting Hg^{2+} to determine the interference effects of other ions during the detection process. Next, competitive experiments were conducted and the results were shown in Figure 4b. Clearly, there was almost none or little change in fluorescence enhancement after the addition of test metal ions. However, the fluorescence intensity was dramatically enhanced upon mixing with Hg^{2+} , thereby exposing the excellent anti-interference ability of the NADP probe. These results implied that the probe can respond to Hg^{2+} with good selectivity and with anti-interference through the changes of fluorescence intensity. Compared with published probes for the detection of Hg^{2+} (Table 1), our probe NADP owns conspicuous advantages, including superior selectivity, anti-interference ability, rapid response time and lower detection limit. More importantly, probe NADP has been successfully applied in cells and zebrafish for fluorescence imaging.

To better understand its use for biological imaging applications, it is very necessary to assess the influence of pH on fluorescence intensity variations for the NADP probe (at 518 nm) in the presence and absence of Hg^{2+} . As displayed in Figure S2a in the Supporting Information, there was almost no change in the fluorescence intensity when the pH ranged from 3 to 11. However, a dramatic enhancement of emission intensity upon treatment with Hg^{2+} was recorded in the pH range of 6.0–11.0, and this was relevant to the physiological pH in organisms. All these results demonstrated that the NADP probe has potential application within biological environments.

Next, the time-dependent fluorescence response of NADP toward Hg^{2+} was explored, because a short response time is also greatly relevant for real time testing of Hg^{2+} in actual samples. As shown in Figure S2b in the Supporting Information, the fluorescence emission intensity response of NADP to Hg^{2+}

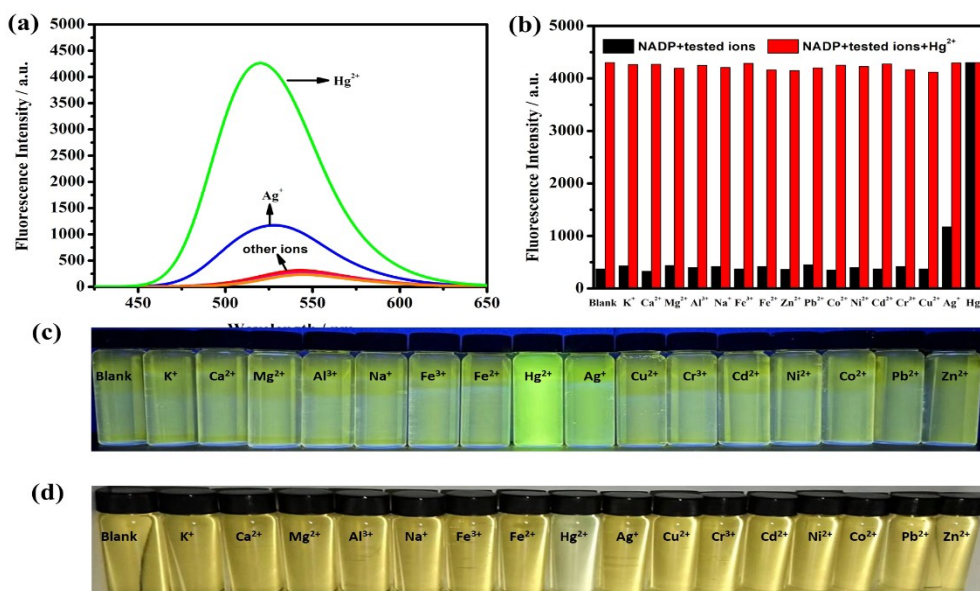
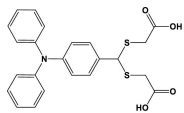
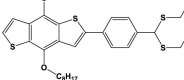
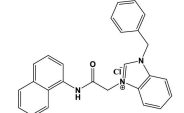
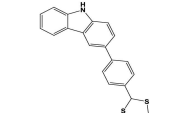
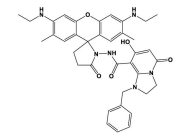
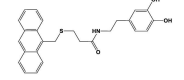
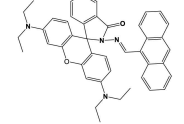
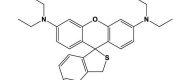
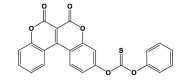
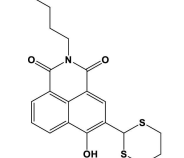


Figure 4. (a) Fluorescence emission spectra of NADP (10 μM) in the presence of various ions. (b) The fluorescence intensity of NADP (10 μM) upon addition of various ions (black bars) and then addition of Hg^{2+} (red bars). (c) Fluorescence color changes for NADP (10 μM) under UV-light (365 nm) in the absence or presence of various ions. (d) Colorimetric changes of NADP (10 μM) under natural light in absence and presence of various ions. The concentrations of metal ions were 10 μM . $\lambda_{\text{ex}} = 400 \text{ nm}$; Slit width = 5/5 nm.

Table 1. Comparison of probe NADP with previously reported selective-Hg²⁺ probes.

| Structure | Excitation/nm | Emission/nm | LOD/nM | Response time/min | Bioimaging application | References |
|---|---------------|-------------|--------|-------------------|-------------------------------|------------|
|  | 368 | 469 | 47 | 3 | No | [62] |
|  | 380 | 459 | 310 | No | Hela cells | [37] |
|  | 300 | 428 | 98 | No | No | [63] |
|  | 346 | 480 | 205 | No | No | [64] |
|  | 537 | 557 | 2570 | 30 | Epithelial cells | [65] |
|  | 360 | 420 | 1100 | No | HepG2 cells | [66] |
|  | 520 | 592 | 873 | No | MIA PaCa-2 and i.e.MCF7 cells | [67] |
|  | 520 | 576 | 2.5 | No | Hela cells | [68] |
|  | 440 | 530 | 85.25 | 15 | No | [69] |
|  | 400 | 518 | 13 | 1.5 | RAW264.7 cells and zebrafish | This work |

increased progressively and instantly, which reached a maximum with the passage of time. In comparison, there were negligible changes in fluorescence emission intensity of NADP during the same period. Consequently, the NADP probe, as a fast fluorescent probe, has great advantages in the terms of real-time detection for Hg²⁺ in living organisms and the environment.

To further explore the practical application of the NADP probe in real samples, it was attached to TLC plates to conveniently and rapidly monitor Hg²⁺. The TLC plates were soaked in DMSO solution with 10 mM of NADP probe and then allowed to dry naturally in air. Then 20 mM Hg²⁺ solution was dripped on the TLC plates. As shown in Figure S3 in the Supporting Information, the color changed from yellow to dark

yellow in sunlight while the fluorescence changed from yellow to green under UV light.

Considering the extremely favorable detection properties of the NADP probe for Hg²⁺, we studied its practical utility by examining intracellular Hg²⁺. Therefore, we used an MTT assay in the presence of RAW264.7 cells to determine a role for the NADP probe in living cells. As depicted in Figure S4 in the Supporting Information, the MTT assay demonstrated the cell viability over 90% after 24 h incubation, demonstrating that the NADP probe has little detrimental effects on living cells. We next performed live cell imaging in RAW264.7 cells, and the results showed that almost no characteristic emission change occurred after incubation with Hg²⁺ (10 μM) for 30 min as depicted in Figure 5b. However, after co-incubation with NADP

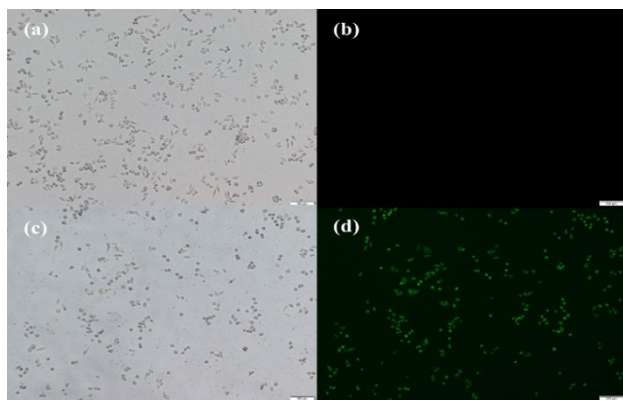


Figure 5. Fluorescence microscopy of NADP applied to RAW264.7 cells: (a) and (b) bright field and fluorescence images of RAW264.7 cells treated with Hg^{2+} ($10\ \mu\text{M}$) alone for 30 min (c) and (d) bright field and fluorescence images of RAW264.7 cells treated with Hg^{2+} ($10\ \mu\text{M}$) for 30 min and further treated with NADP ($10\ \mu\text{M}$) for an additional 30 min, respectively.

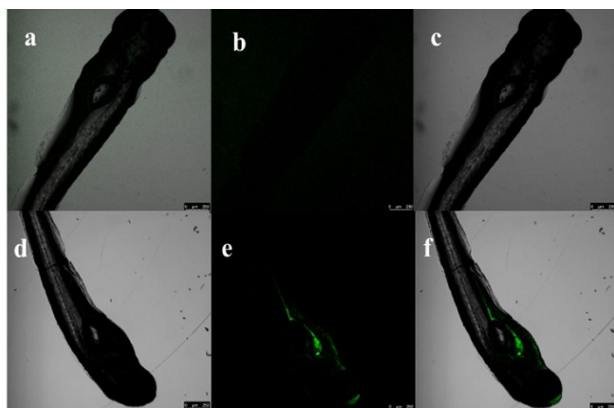


Figure 6. (a–c) Zebrafish was treated with Hg^{2+} ($10\ \mu\text{M}$) for 30 min. (d–f) Subsequent addition of NADP ($10\ \mu\text{M}$) for 1 h.

($10\ \mu\text{M}$) for 30 min, the brightness of the green fluorescence gradually emerged and was enhanced Figure 5d. These results demonstrated that the NADP probe has the ability to detect Hg^{2+} in living cells.

To further investigate the unrivalled potential of NADP responding to Hg^{2+} in the terms of fluorescent bioimaging, four-day-old zebrafish was selected as the research model of bioluminescence imaging. As exhibited in Figure 6, there was no fluorescent emission in zebrafish with the treatment of Hg^{2+} for 30 min. However, a remarkable green fluorescent emission was observed in stomach of zebrafish after co-incubation with NADP. These experimental results forcefully denoted that NADP could successfully detect Hg^{2+} in zebrafish with the changing of the fluorescent colors from colorless to green.

3. Conclusion

A 1,8-naphthalimide-based bright-green emission probe NADP for the detection of Hg^{2+} based on a Hg^{2+} -promoted deprotection reaction has been developed. Our data indicates that

the NADP probe has several advantages over other reported probes, such as high sensitivity and excellent selectivity, applicable to wide pH range, and a low detection limit down to $13\ \text{nM}$ for Hg^{2+} recognition. More importantly, the probe is not only cell permeable with low cytotoxicity, but also is a useful tool for the visualization of Hg^{2+} in living cells and zebrafish. Taken together, the NADP probe has great potential for the detection of Hg^{2+} in both the environment and living organic systems.

Experimental Section

The synthetic procedure for NADP was clearly described in Scheme S1 in the Supporting Information. NADP was designed on the basis of the deprotected reaction of dithioacetal between NA-CHO and the corresponding thiol compounds triggered by Hg^{2+} . During the catalysis of $\text{BF}_3 \cdot \text{Et}_2\text{O}$, the condensation reaction of NA-CHO and 1,3-dimercaptopropane in anhydrous CH_2Cl_2 at room temperature yielded the sensor NADP, which was structurally characterized and validated with ^1H NMR, ^{13}C NMR, and HRMS spectroscopy (see Figures S5–S7 in the Supporting Information).

Acknowledgements

The project was supported by the Yong Science Foundation of Shandong Academy of Science (No. 2020QN0018).

Conflict of Interest

The authors declare no competing financial interests.

Keywords: cell imaging · deprotection reactions · mercury ions · naphthalimide · fluorescent probes

- [1] P. R. M. Araujo, C. M. Biondi, C. W. A. do Nascimento, F. B. V. da Silva, W. R. da Silva, F. L. da Silva, D. K. D. Ferreira, *Chemosphere* **2021**, *266*, 12.
- [2] M. O. Asare, J. O. Afriyie, *Water Air Soil Pollut.* **2021**, *232*, 22.
- [3] P. P. Bhav, R. Shrestha, in *Global Challenges in Energy and Environment* (Eds.: V. Sivasubramanian, S. Subramanian), Springer-Verlag Singapore Pte Ltd, Singapore, **2020**, pp. 77–88.
- [4] P. Charvat, L. Klimes, J. Pospisil, J. J. Klemes, P. S. Varbanov, *J. Cleaner Prod.* **2020**, *267*, 11.
- [5] A. Jedruch, L. Falkowska, D. Saniewska, M. Durkalec, A. Nawrocka, E. Kalisinska, A. Kowalski, J. M. Pacyna, *Ambio* **2021**, *50*, 1698–1717.
- [6] K. Y. Liu, Q. R. Wu, L. Wang, S. X. Wang, T. H. Liu, D. Ding, Y. Tang, G. L. Li, H. Z. Tian, L. Duan, X. Wang, X. W. Fu, X. B. Feng, J. M. Hao, *Environ. Sci. Technol.* **2019**, *53*, 8938–8946.
- [7] S. J. Liu, X. D. Wang, G. L. Guo, Z. G. Yan, *J. Environ. Manage.* **2021**, *277*, 12.
- [8] Ramlan, M. Basir-Cyio, M. Napitupulu, T. Inoue, A. Anshary, Mahfudz, Irun, M. Rusydi, Golar, Sulbadana, R. Bakri, *Int. J. Environ. Sci. Technol.* **2021**, DOI: 10.1007/s13762-021-03345-8.
- [9] Z. C. Song, C. Wang, L. Ding, M. Chen, Y. X. Hu, P. Li, L. M. Zhang, X. B. Feng, *J. Cleaner Prod.* **2021**, *288*, 10.
- [10] X. C. Tang, X. L. Wu, P. H. Xia, T. Lin, X. F. Huang, Z. M. Zhang, J. C. Zhang, *Environ. Sci. Pollut. Res.* **2021**, *28*, 48837–48850.
- [11] V. L. Cariccio, A. Sama, P. Bramanti, E. Mazzon, *Biol. Trace Elem. Res.* **2019**, *187*, 341–356.
- [12] F. Chirico, E. Scoditti, C. Viora, N. Magnavita, *Appl. Sci.-Basel* **2020**, *10*, 14.

- [13] D. T. Hill, M. Petroni, D. A. Larsen, K. Bendinskas, K. Heffernan, N. Atallah-Yunes, P. J. Parsons, C. D. Palmer, J. A. MacKenzie, M. B. Collins, B. B. Gump, *Environ. Res.* **2021**, *193*, 11.
- [14] X. F. Hu, M. Lowe, H. M. Chan, *Environ. Res.* **2021**, *193*, 11.
- [15] N. Magnavita, M. Sabatelli, E. Scoditti, F. Chirico, *Appl. Sci.-Basel* **2020**, *10*, 9.
- [16] R. Pamphlett, P. A. Doble, D. P. Bishop, *PLoS One* **2021**, *16*, 16.
- [17] C. J. Wu, J. B. Wang, J. J. Shen, C. Bi, H. W. Zhou, *Sens. Actuators B* **2017**, *243*, 678–683.
- [18] C. G. Chen, N. Vijay, N. Thirumalaivasan, S. Velmathi, S. P. Wu, *Spectrochim. Acta Part A* **2019**, *219*, 135–140.
- [19] S. S. Dai, Z. M. Yang, Y. D. Tong, L. Chen, S. Y. Liu, R. Pan, Y. B. Li, C. J. Zhang, Y. R. Liu, Q. Y. Huang, *J. Hazard. Mater.* **2021**, *407*, 8.
- [20] D. L. Haskins, M. K. Brown, R. B. Bringolf, T. D. Tuberville, *Sci. Total Environ.* **2021**, *755*, 9.
- [21] X. Y. Huang, H. M. Yu, X. M. Zhao, X. Guo, Y. C. Ye, Z. Xu, *Front. Environ. Sci.* **2021**, *9*, 12.
- [22] M. Mohan, M. S. S. Chandran, E. V. Ramasamy, *Reg. Stud. Mar. Sci.* **2021**, *44*, 12.
- [23] Natasha, M. Shahid, S. Khalid, I. Bibi, J. Bundschuh, N. K. Niazi, C. Dumat, *Sci. Total Environ.* **2020**, *711*, 22.
- [24] U. A. Rebolledo, F. Paez-Osuna, R. Fernandez, *Environ. Pollut.* **2021**, *271*, 11.
- [25] K. S. Vieira, J. A. B. Neto, M. A. C. Crapez, C. Gaylarde, B. D. Pierri, M. Saldana-Serrano, A. C. D. Bairy, D. J. Nogueira, E. M. Fonseca, *Mar. Pollut. Bull.* **2021**, *166*, 10.
- [26] M. Zupancic, M. Sustersic, S. Bavec, M. Gosar, *Environ. Geochem. Health* **2021**, *43*, 3505–3531.
- [27] R. Gras, J. Luong, R. A. Shellie, *ACS Earth Space Chem.* **2018**, *2*, 471–478.
- [28] Y. Y. Su, K. L. Xu, Y. Gao, X. D. Hou, *Microchim. Acta* **2008**, *160*, 191–195.
- [29] D. Martin-Yerga, A. Costa-Garcia, *Curr. Opin. Electrochem.* **2017**, *3*, 91–96.
- [30] Z. L. Sun, J. J. Du, C. Y. Jing, *J. Environ. Sci.* **2016**, *39*, 134–143.
- [31] J. J. Du, L. Jiang, Q. Shao, X. G. Liu, R. S. Marks, J. Ma, X. D. Chen, *Small* **2013**, *9*, 1467–1481.
- [32] Y. G. Yin, M. Chen, J. F. Peng, J. F. Liu, G. B. Jiang, *Talanta* **2010**, *81*, 1788–1792.
- [33] L. Y. Chen, S. J. Park, D. Wu, H. M. Kim, J. Yoon, *Chem. Commun.* **2019**, *55*, 1766–1769.
- [34] X. H. Cheng, S. H. Qu, L. Xiao, W. N. Li, P. He, *J. Photochem. Photobiol. A-Chem.* **2018**, *364*, 503–509.
- [35] Y. H. Hou, M. H. Yan, Q. F. Wang, Y. F. Wang, Y. F. Xu, Y. T. Wang, H. Y. Li, H. Wang, *Food Anal. Methods* **2017**, *10*, 1931–1939.
- [36] X. J. Jiao, C. Liu, S. He, L. C. Zhao, X. S. Zeng, *Dyes Pigm.* **2019**, *160*, 86–92.
- [37] T. H. Leng, Y. W. Ma, G. Y. Chen, *J. Photochem. Photobiol. A-Chem.* **2018**, *353*, 143–149.
- [38] S. D. Liu, D. Feng, L. W. Zhang, H. Song, Y. Wang, X. Zhang, Q. J. Zhao, L. X. Chen, *Spectrochim. Acta Part A* **2020**, *243*, 6.
- [39] J. Tang, H. Wu, S. Yin, Y. F. Han, *Tetrahedron Lett.* **2019**, *60*, 541–546.
- [40] J. L. Wang, W. L. Li, L. P. Long, *Sens. Actuators B* **2017**, *245*, 462–469.
- [41] Q. M. Wang, L. Jin, W. L. Wang, T. X. Hu, C. Chen, *J. Lumin.* **2019**, *209*, 411–419.
- [42] X. Yuan, T. H. Leng, Z. Q. Guo, C. Y. Wang, J. Z. Li, W. W. Yang, W. H. Zhu, *Dyes Pigm.* **2019**, *161*, 403–410.
- [43] X. J. Zhu, S. T. Fu, W. K. Wong, H. P. Guo, W. Y. Wong, *Angew. Chem. Int. Ed.* **2006**, *45*, 3150–3154; *Angew. Chem.* **2006**, *118*, 3222–3226.
- [44] X. J. Zhu, S. T. Fu, W. K. Wong, W. Y. Wong, *Tetrahedron Lett.* **2008**, *49*, 1843–1846.
- [45] V. Bhardwaj, V. M. Nurchi, S. K. Sahoo, *Pharmaceuticals* **2021**, *14*, 45.
- [46] V. Tekuri, S. K. Sahoo, D. R. Trivedi, *Spectrochim. Acta Part A* **2019**, *218*, 19–26.
- [47] J. P. Nandre, S. R. Patil, S. K. Sahoo, C. P. Pradeep, A. Churakov, F. B. A. Yu, L. X. Chen, C. Redshaw, A. A. Patil, U. D. Patil, *Dalton Trans.* **2017**, *46*, 14201–14209.
- [48] E. Bozkurt, H. I. Gul, *Sens. Actuators B* **2018**, *255*, 814–825.
- [49] E. Bozkurt, H. I. Gul, *Inorg. Chim. Acta* **2020**, *502*, 7.
- [50] D. Giri, A. Bankura, S. K. Patra, *Polymer* **2018**, *158*, 338–353.
- [51] Y. Guo, J. An, H. Y. Tang, M. J. Peng, F. Suzenet, *Mater. Res. Bull.* **2015**, *63*, 155–163.
- [52] L. Y. Huang, Z. T. Yang, Z. L. Zhou, Y. Q. Li, S. P. Tang, W. P. Xiao, M. Hu, C. Peng, Y. X. Chen, B. Gu, H. T. Li, *Dyes Pigm.* **2019**, *163*, 118–125.
- [53] J. H. Kim, H. J. Kim, S. H. Kim, J. H. Lee, J. H. Do, H. J. Kim, J. H. Lee, J. S. Kim, *Tetrahedron Lett.* **2009**, *50*, 5958–5961.
- [54] C. E. Wang, L. Z. Wang, S. M. Fang, D. W. Qin, J. H. Zhou, G. Yang, S. S. Jin, H. D. Duan, *Res. Chem. Intermed.* **2019**, *45*, 2045–2063.
- [55] D. Xu, L. J. Tang, M. Y. Tian, P. He, X. M. Yan, *Tetrahedron Lett.* **2017**, *58*, 3654–3657.
- [56] J. Lv, F. Wang, T. W. Wei, X. Q. Chen, *Ind. Eng. Chem. Res.* **2017**, *56*, 3757–3764.
- [57] J. Ding, H. Y. Li, C. Wang, J. Yang, Y. J. Xie, Q. Peng, Q. Q. Li, Z. Li, *ACS Appl. Mater. Interfaces* **2015**, *7*, 11369–11376.
- [58] M. Caricato, G. Trucks, M. Frisch, K. B. Wiberg, *Abstr. Pap. Am. Chem. Soc.* **2009**, *238*, 1.
- [59] T. Lu, F. W. Chen, *J. Comput. Chem.* **2012**, *33*, 580–592.
- [60] X. J. Zhang, Y. F. Xu, P. Guo, X. H. Qian, *New J. Chem.* **2012**, *36*, 1621–1625.
- [61] L. J. Tang, S. L. Ding, X. R. Zhang, K. L. Zhong, S. H. Hou, Y. J. Bian, *J. Photochem. Photobiol. A-Chem.* **2017**, *340*, 15–20.
- [62] D. L. Hu, S. J. Liao, X. Chen, J. C. Du, K. Dawood, S. Chauhan, C. Gao, W. Li, *Bull. Korean Chem. Soc.* **2020**, *41*, 686–690.
- [63] L. Y. Wang, C. H. Lou, M. Zhao, B. Zhao, H. P. Zhao, W. H. Ma, A. Q. Wang, X. Wang, N. Wang, Y. F. Li, *Inorg. Chem. Commun.* **2021**, *129*, 6.
- [64] J. M. Pan, J. Ma, L. Liu, D. H. Li, Y. T. Huo, H. Liu, *J. Photochem. Photobiol. A-Chem.* **2021**, *416*, 9.
- [65] B. U. Gauthama, B. Narayana, B. K. Sarojini, N. K. Suresh, Y. Sangappa, A. K. Kudva, G. Satyanarayana, S. V. Raghu, *Microchem. J.* **2021**, *166*, 10.
- [66] W. J. Feng, Q. Xia, H. Y. Zhou, Y. Ni, L. L. Wang, S. Jing, L. Li, W. Ji, *Talanta* **2017**, *167*, 681–687.
- [67] F. Cicekbilek, B. Yilmaz, M. Bayrakci, O. Gezici, *J. Fluoresc.* **2019**, *29*, 1349–1358.
- [68] A. L. Luo, Y. J. Gong, Y. Yuan, J. Zhang, C. C. Zhang, X. B. Zhang, W. H. Tan, *Talanta* **2013**, *117*, 326–332.
- [69] Y. H. Jiang, H. W. Li, R. F. Chen, W. Liu, C. Y. Chen, Z. G. Li, W. S. Liu, *Spectrochim. Acta Part A* **2021**, *251*, 9.

Manuscript received: July 30, 2021

Revised manuscript received: September 27, 2021